2-2009

The Mechanical Properties of Individual, Electrospun Fibrinogen Fibers

Christine C. Helms
University of Richmond, chelms@richmond.edu

Corentin Coulais

Manoj Namboothiry

David L. Carroll

Roy R. Hantgan

See next page for additional authors

The mechanical properties of individual, electrospun fibrinogen fibers

Carlisle, R.C. [1], Coulais, C.[2], Namboothiry, M.[1], Carroll, D.[1], Hantgan, R.R.[3], Guthold, M.[1,*]

[1] Department of Physics, Wake Forest University, Winston-Salem, NC 27109, USA
[2] Current address: Ecole Normale Supérieure de Lyon, Université Claude Bernard Lyon 1, France
[3] Department of Biochemistry, Wake Forest University School of Medicine, Winston-Salem, NC 27157, USA

* Corresponding author

Abstract

We used a combined atomic force microscope (AFM)/fluorescence microscope technique to study the mechanical properties of individual, electrospun fibrinogen fibers in aqueous buffer. Fibers (average diameter 208 nm) were suspended over 12 μm-wide grooves in a striated, transparent substrate. The AFM, situated above the sample, was used to laterally stretch the fibers and to measure the applied force. The fluorescence microscope, situated below the sample, was used to visualize the stretching process. The fibers could be stretched to 2.3 times their original length before breaking; the breaking stress was $22 \cdot 10^6$ Pa. We collected incremental stress-strain curves to determine the viscoelastic behavior of these fibers. The total stretch modulus was $16 \cdot 10^6$ Pa and the relaxed, elastic modulus was $6.7 \cdot 10^6$ Pa. When held at constant strain, electrospun fibrinogen fibers showed a fast and slow stress relaxation time of 3 and 56 seconds.
Our fibers were spun from the typically used 90% 1,1,1,3,3,3-hexafluoro-2-propanol (90-HFP) electrospinning solution and resuspended in aqueous buffer. Circular dichroism spectra indicate that alpha-helical content of fibrinogen is ~70% higher in 90-HFP than in aqueous solution.
These data are needed to understand the mechanical behavior of electrospun fibrinogen structures. Our technique is also applicable to study other, nanoscopic fibers.

(Abstract: 199 words)

Keywords: AFM, fluorescence, biomimetic material, fibrinogen, mechanical properties, viscoelasticity.

Introduction

Fibrinogen is a highly abundant plasma protein with molecular mass 340,000 daltons. It consists of six polypeptide chains; 2 Aα, 2 Bβ and 2 γ chains which are bound together by 29 disulfide bonds [1]. Fibrinogen has a tri-nodular shape, with two nodules (the D-domains) at either end and one nodule (the E-domain) in the center. The nodules are connected by two 17 nm long coiled coils consisting of three alpha helices. Fibrinogen is about 45 nm in length and 4.5 nm in diameter (Fig. 1A). In the event of injury to the vasculature, activated thrombin cleaves two fibrinopeptides A (16 residues) and two fibrinopeptides B (14 residues) from the amino termini of the Aα and Bβ chains (located at the central E-domain), thus converting fibrinogen into fibrin. Fibrin then polymerizes spontaneously into a meshwork of fibrin fibers which comprises the main structural component of a blood clot [2]. Thrombin-activated factor XIII forms covalent γ–γ and α–α crosslinks between the γ– and α-chains of neighboring fibrin molecules, which further stabilizes the fibrin network. The fibrin fibers in this network have a wide range of diameters with an average of about 60 nm [3]. The initial task of the fibrin fiber network is stemming the flow of blood to prevent blood loss; subsequently, it plays a significant role in controlling the enzymatic processes of wound healing [4].
Aside from these naturally formed fibrin fibers, fibrinogen can also be spun electrostatically into nanoscopic fibers. In this technique, termed "electrospinning", fibers are formed from a thin stream of concentrated protein solution emerging from a syringe (Fig. 1B). The emerging protein solution forms fibers as it is subjected to a high electric field between the syringe needle and a grounding plate. The fibers are deposited on the grounding plate. Patented in 1934 for textile use, electrospinning has recently received renewed interest, as electrospun nanofibers may be ideal candidates for numerous, novel biomedical applications such as tissue engineering scaffolds, wound dressings, coatings, or drug delivery vehicles [5]. In addition to biomedical applications, electrospun fibers may also find uses in novel polymer composites [5, 6].

Electrospun fibrinogen fibers, in particular, might be attractive candidates for biomedical applications, due to their biocompatibility. The immunogenicity of fibrinogen is low, as it does not cause inflammation and it does not result in toxic degradation products [7]. Moreover, fibrinogen can be used autologously which nearly eliminates the risk of an immune response. Thus, fibrinogen fibers should be well-suited for applications in humans. Fibrinogen also is a natural choice to form artificial fibers, since one of its main physiological purposes is to form the fibrin fibers that comprise the structural scaffold of a blood clot. Fibrin(ogen) regulates many processes in tissue repair and regeneration, and angiogenesis [4]; electrospun fibrinogen fibers may, thus, be utilized to regulate some of these tissue rebuilding processes, as well [8, 9]. Fibrinogen scaffolds have been shown to support cell proliferation and to promote cell interaction [10]. Fibrinogen fibers can be dissolved again by the natural clot dissolution process (fibrinolysis), and are, therefore easily 'degradable' in the body. Scaffolds constructed from electrospun fibrinogen fibers have recently been tested successfully in urinary tract tissue engineering [11].
When designing structures or devices, such as tissue scaffolds, wound dressings or drug delivery particles, it is important that the mechanical properties of the device match the requirements of the task at hand, for example a device may have to be stiff, or compliant.

The overall mechanical properties of any structure built from fibers depend on three distinct quantities: i) the architecture of the structure, ii) the properties of the single fibers comprising the structure and iii) the junctions between the fibers comprising the structure. All three need to be known so that a structure with predictable mechanical properties can be designed.
Addressing item ii), we developed a microscopy-based technique to determine the mechanical properties of individual, electrospun fibrinogen fibers. This technique should also be widely applicable to investigate other nanoscopic fibers.

Materials and Methods

Substrate Preparation

Preparation of the striated substrate is based on soft lithography and MIMIC (micromoulding in capillaries) [12]. Briefly, a PDMS (polydimethylsiloxane) stamp was prepared by pouring dimethylsiloxane plus catalyst (Sylgard, Dow Corning Corp, Midland, MI) onto a SU-8-silicon master grid (gift or Prof. Superfine, University of North Carolina, Chapel Hill) in a petri dish. The polymer was cured at 70°C for one hour. The PDMS stamp was removed from the master and pressed into a 10 μl drop of Norland Optical Adhesive-81 (NOA-81, Norland Products, Cranbury, NJ) on top of a 60mm x 24mm, #1, microscope cover slide (VWR International, West Chester, PA). The NOA-81 was cured for 70 seconds with UV light (365 nm setting, UVP 3UV transilluminator, Upland, CA) and the stamp was removed. The substrate pattern we used had 12 μm wide and 6 μm deep channels and 8 μm wide ridges.

Formation of Electrospun Fibrinogen Fibers

Our procedures used for electrostatic spinning of fibrinogen fibers, schematically depicted in Fig. 1B, are based on those developed by Wnek et al. [13]. A polymer solution, comprised of 100 mg/ml lyophilized bovine fibrinogen, (Sigma-Aldrich Chemical Co), 9 parts 1,1,1,3,3,3-hexafluoro-2-propanol (HFP, Sigma-Aldrich) and 1 part minimum essential medium (MEM), (10x MEM, Gibco, Invitrogen cell culture) was prepared. SDS PAGE showed that this fibrinogen sample was about 79% pure, and that there was no detectable crosslinking under our experimental conditions (data not shown). The solution was filled into a 1 ml volume, 4 mm diameter syringe (Becton-Dickinson, Franklin Lakes, New Jersey). The syringe was outfitted with a 23x¾ -gauge butterfly and tubing infusion set needle (Abbott Laboratories, North Chicago, IL) and was placed in the syringe pump (NE-1000 Programmable Syringe Pump, New Era Pump System, Inc,Wantagh, New-York) and dispensed at a rate of 1.9 ml/hr. A voltage of 22 kV was applied across the needle and the substrate (grounding plate), which was placed at a distance of 12.5cm or 20cm from the needle. The grounding plate consisted of the cover glass (with the striated surface) connected to ground with an alligator clip. Between 5 μl and 15 μl of polymer solution was dispensed onto each striated cover glass surface.

Labeling and Resuspension of Fibers

After fiber formation, the fibers were labeled with 24 nm**,** yellow-green carboxyl fluorescent beads (Invitrogen, Fluospheres, Carlsbad, CA) diluted 1/10000 in fiber buffer-1 (10mM Hepes, 140mM NaCl, pH 7.4). A 100 μl drop of the diluted bead solution was placed on the electrospun fiber coated cover slide for 10 minutes; the slide was then rinsed with fiber buffer-2 (10mM Hepes, 140mM NaCl, 5 mM $CaCl_2$, pH 7.4) and stored in fiber buffer-2.

Combined Atomic Force Microscopy (AFM)/Fluorescence Microscopy

The mechanical manipulations of the electrospun fibers were performed with our combined AFM and optical microscope instrument (Fig. 2) [14, 15]. The AFM (Topometrix Explorer, Veeco Instruments, Woodbury, NY) fits our custom-built stage of the Zeiss Axiovert 200 inverted microscope (Zeiss, Göttingen, Germany). The stage is designed so that the AFM tip can be aligned with the objective lens and it also permits the sample to be moved independently of the AFM tip and the objective lens. This design allows us to position any area of the sample between the AFM tip and the objective lens. A Hamamatsu EM-CCD C9100 Camera (Hamamatsu Photonics KK, Japan) and IPLab software (Scanalytics, Fairfax, VA) were used to collect and analyze the fluorescence microscopy images and movies. For the AFM imaging and manipulation experiments, silicon cantilevers (Young's modulus, $E = 1.69 \times 10^{11}$ Pa) with a rectangular cross-section were used (NSC12 without Al, spring constant, k = 0.3 N/m, length, l = 330 μm; width, w = 34 μm; thickness, t = 1.3 μm; tip height, h = 15 μm; MikroMasch, Wilsonville, OR).

Fiber Manipulations and Force Calculations

Stress is defined as $\sigma = F/A$, where F is the applied force and A is the cross-sectional area of the fiber. We used the cross-section of the initial, unstretched fiber in our calculations, i.e. we used the so-called engineering stress in this paper. Strain is defined as $\varepsilon = \Delta L/L_{init}$, where $\Delta L = L' - L_{init}$ is the change in fiber length; L' and L_{init} are the lengths of the stretched and unstretched fiber, respectively.

A nanoManipulator (3^{rd} Tech, Chapel Hill, NC), was used to control the AFM tip movement in the x-, y- and z- direction. After aligning the AFM tip with the objective lens, the sample was moved until a fiber was centered in the field of view. The tip was then lowered onto a ridge of the striated substrate. Once the tip was on the surface, the nanoManipulator software was used to raise the tip in the z direction (away from the surface) and to move the tip next to the fiber in the center of a groove on the striated surface. The z-position of the tip was then further adjusted, so that the point of the tip was at the same height as the fiber. This last step was done to assure that the lever arm of the lateral force measurement would be equal to h + t/2, where h is the tip height and t is the thickness of the cantilever (see equation (2) for K_C below).

The fiber was then stretched by laterally moving the tip, along the groove, into the fiber. Fibers suspended over such a surface provide an easy to analyze geometry for mechanical manipulations and for collecting stress-strain curves (Fig. 2C). Fig. 2D shows a movie sequence of a typical fiber stretching experiment.

The acquisition of the fiber stress-strain data involved a series of steps. The "left – right" photocurrent data (which corresponds to the twist of the cantilever, see Fig. 3) was

recorded by the nanoManipulator during the manipulation. The left – right photocurrent signal, I_l, was converted into lateral force (in Newtons) by multiplying it with the lateral force conversion factor K_C;

$$F_l = K_C \cdot I_l \quad (1).$$

K_C can be determined via cantilever beam mechanics,

$$K_C = \frac{Ewt^3}{6l^2(h + t/2)} \cdot S_n \quad (2),$$

where E, w, t, and l are the Young's modulus, the width, the thickness and length of the cantilever, h is the height of the tip. S_n is the 'normal sensor response', i.e. the conversion of normal cantilever deflection to top – bottom photocurrent. The length and width of the cantilever and the height of the tip were determined for each cantilever individually with the optical microscope. The resonance frequency of the cantilever was used to determine the thickness of the cantilever via

$$f = 0.276 \cdot \sqrt{\frac{Ewt^3}{\rho(\pi \cdot h^3 \cdot l^3 + 0.2832 wtl^4)}} \quad (3),$$

where $\rho = 2330$ kg/m^3 is the density of silicon. The error in K_C, as determined from the beam mechanics method, can be estimated from the uncertainties in the quantities: l, 2%; w, 2%; t, 10%; h, 10%; and S_n, 10%, yielding an overall error in K_C of about 56%. This method of determining K_C (based on cantilever beam mechanics) was double-checked with the glass fiber calibration method, in which K_C is determined by bending a small glass fiber with known dimensions and Young's modulus [16]. The error in the glass fiber calibration method is dependent upon the properties of the glass fiber (radius, length and Young's modulus) and the cantilever deflection, Δy, resulting in an overall error in K_C of about 26%. For details of both calibration methods, see [16]. The normal sensor response, S_n, was acquired before or after each manipulation experiment.

The cross-sectional area of the fibrinogen fibers, A, needed to calculate the stress applied to the fibers, $\sigma = F/A$, was determined concurrently by imaging the fiber on the ridge with the AFM. The diameter, D, was determined from the height data and used to calculate the cross-sectional area $A = \pi(D/2)^2$. The error in D is about 10%.

The diameter of the fibers (~ 200 nm) could not be determined via optical microscopy, because it is below the resolution limit, $d = (0.61*\lambda)/N.A \sim 430$ nm, of our objective lens (40x, N.A. = 0.75, $\lambda \sim 525$ nm)."

Circular Dichroism (CD) Spectra

CD spectra were taken to compare the secondary structure of fibrinogen in aqueous solution, and in electrospinning solution. The CD spectra were taken for human fibrinogen solutions prepared in phosphate buffered saline (PBS, Sigma-Aldrich) and HFP. A total volume of 300 μl of fibrinogen solution was prepared in PBS at a concentration of 40.4 mg/ml fibrinogen (Enzyme Research Laboratories, South Bend, IN). 300 μl was also prepared in the HFP solution at a fibrinogen concentration of 32.7 mg/ml. Aliquots of each sample were diluted ~140-fold in their respective buffers prior to obtaining UV absorbance data in a BioRad SmartSpec Plus spectrophotomer and circular dichroic spectral data in a JASCO Model 720 spectropolarimeter. Both samples exhibited absorbance maxima near 280 nm, enabling calculation of the fibrinogen concentrations

(0.292 mg/ml in PBS; 0.285 mg/ml in HFP) using a weight/volume extinction coefficient of 1.6 ml/mg-cm. CD spectra were taken with each sample from 195 nm to 360 nm for the HFP-fibrinogen solution and PBS-fibrinogen solution. Spectra were also taken for PBS and HFP solutions to be used as baseline measurements. Calculations of mean residue ellipticity, [Θ], versus wavelength were obtained using a mean residue weight of 114.7 for fibrinogen, calculated from its molecular weight (340,000) and total number of residues [17].

Results

Fiber Morphology

Electrospun fibrinogen fibers were formed from a 100 mg/ml fibrinogen solution. Fibers were collected on either a regular cover glass substrate or a striated substrate with 12 μm wide and 6 μm deep grooves and 8 μm wide ridges prepared from optical adhesive. The fibers, which were formed on the cover glass without ridges, were imaged with the AFM in air (Fig. 4). The fibers had a relatively smooth, uniform appearance and an average radius of 208 ± 84 nm (22 fibers, values are stated ± their standard deviation), in agreement with published data [18].

Fiber extensibility and Breaking Strain

We then tested the mechanical properties of single, electrospun fibrinogen fibers in aqueous solution. Fibrinogen fibers were electrospun on the striated substrate using the same 100 mg/ml fibrinogen solution as above, and re-suspended in fiber buffer-2. As seen in the fluorescence images in Fig. 5 A-D, taken from underneath the sample, the fibers are suspended over the 12 μm wide and 6 μm deep grooves and anchored on the 8 μm wide ridges. The AFM tip, situated above the sample, was used to stretch the fiber. Fig. 5 depicts the extensibility measurements of the fibers. Extensibility is defined as the maximum strain $\varepsilon_{max,}$ at which a fiber will break. This is an important fiber property, as it determines the ultimate failure of a fiber. The extensibility of the fibers was tested by using the AFM tip to stretch the fibers parallel to the ridges until they broke (see Fig. 5A-D). The stretch rate for those experiments was between 250 and 425 nm/s. The fibers we studied were usually firmly (though non-specifically) anchored on the ridges, as we have seldomly seen them detach at the anchoring point when stretching them. Moreover, since we obtain images and movies of each manipulation, we can ascertain that the fibers are not slipping at the anchoring points. Fig. 5 E shows a histogram of the extensibility of 34 electrospun fibrinogen fibers. The average extensibility of the hydrated electrospun fibrinogen fibers was $\varepsilon_{max} = 1.3 \pm 0.4$; that is, electrospun fibrinogen fibers can be stretched to 2.3 times their initial length before breaking.

This extensibility is comparable to that of the high-extensibility natural fibers, and it is larger than that of the low-extensibility, natural fibers (see table 1). However, it is still less than the extremely large extensibility of hydrated, naturally formed, partially crosslinked and non-crosslinked fibrin fibers ($\varepsilon_{max} = 3.32$ and $\varepsilon_{max} = 2.26$, respectively). Naturally formed fibrin fibers are the most stretchable protein fibers in nature [14].

Fig. 5 F shows a histogram of the maximum stress, σ_{max}, at which the fibers ruptured. This quantity is important, because it is a measure of how much force a fiber can sustain, before breaking. The average maximum stress of the hydrated electrospun fibrinogen fibers formed at 100 mg/ml concentration was σ_{max} = 22 MPa.

Fiber Viscoelastic Properties

To determine the stiffness and several viscoelastic properties of electrospun fibrinogen fibers, we collected incremental stress-strain curves on eight fibers. In this measurement, the fiber is first strained (stretched) a certain amount, then held at that particular strain for a period of time. During this holding time, the fiber relaxes, which means that the force (stress) to hold the fiber at that position decreases, usually exponentially, to a certain value. The stress does not decay to zero, but rather approaches a non-zero stress value asymptotically. The fiber is then strained some more and held at that new strain for some time. During this holding time, the fiber again relaxes to a certain stress value. This incremental stretching process is repeated until the fiber ruptures. Several key insights about the mechanical behavior and performance can be gained from such incremental stress strain curves. 1) Viscoelasticity. It can be determined if a fiber is mainly elastic, mainly viscous or viscoelastic. Totally elastic fibers (e.g. a perfect rubber band) would not relax at all; and totally viscous fibers (e.g. perfect play dough) would relax completely to zero stress during each holding period. Most polymeric fibers show viscoelastic behavior, i.e. a mixture of viscous and elastic behavior. Incremental stress-strain curves can be used to demonstrate that a polymer behaves viscoelastically and to separate the elastic and viscous behavior. 2) Relaxation time(s). Stress relaxation indicates viscous behavior and the rate(s) at which the stress decays at the holding points provides the relaxation times. The relaxation times may provide information about time scales of internal rearrangements of the fibers. 3) Elastic modulus. When plotting the relaxed stress values versus the strain, the slope is the elastic (or Young's) modulus of the fiber. This corresponds to the elastic 'stiffness' of fibers, i.e. the stiffness for slow manipulations. 4) The total stretch modulus. When plotting the total (unrelaxed) stress versus the strain, the slope is the total stretch modulus. This modulus is speed (or frequency)-dependent. Because our experimental set-up currently has limited speed (frequency) range in the lateral force direction, we determined the total modulus at only one speed.

Fig. 6 shows a typical incremental stress-strain curve of electrospun fibrinogen fibers. Fig. 6 A is a graph of strain versus time; the fiber was first stretched to $\varepsilon = 0.27$ and held for 84s, the strain was then increased to $\varepsilon = 0.51$ and held for 74 s, the strain was further increased to $\varepsilon = 0.94$ and held for 80 s, the fiber then ruptured on the next incremental strain increase. Fig. 6 B shows a plot of stress versus time of the same fiber manipulation. The time axis in Figs. 6 A & B is the same. It can be seen that the stress relaxes during the time periods at which the fiber was held at constant strain; however, it does not relax to zero. This is indicative of viscoelastic behavior.

Fig. 6 C shows the complete stress versus strain curve of this manipulation (in gold) for this fiber. The top curve (solid black line) shows the total stress versus the strain, the three dips at $\varepsilon = 0.27$, 0.51 and 0.94 occur when the fiber is held at constant strain. The average slope of this curve corresponds to the average total modulus for hydrated, electrospun fibrinogen fibers (averaged over the entire strain region). It has a mean value

of $(16 \pm 8) \cdot 10^6$ Pa (mean ± standard deviation for incremental stress strain curves of N = 8 fibers). The dashed line corresponds to the relaxed, elastic component of the fiber. The slope of this curve corresponds to the elastic (Young's) modulus and has a mean value of $(6.7 \pm 2.7) \cdot 10^6$ Pa.

We also attempted to fit the clamped, cylindrical beam equation $x = \frac{FL^3}{3\pi ED^4}$ [19], to our low strain data ($\varepsilon \leq 0.1$), for which this equation is valid (x is the deflection, F is the applied force, L, E and D are the length, Young's modulus and diameter of the fiber). However, the noise and uncertainty of our data in this small strain, small force regime ($\varepsilon \leq 0.1$, F ≤ 10 nN) were too large to obtain a reliable measurement of the Young's modulus by the clamped beam equation.

Aside from the total and elastic modulus, the incremental stress-time curves can also be used to extract the time scales for fiber relaxation. Fig. 7 shows a stress relaxation curve. Two exponentials, modeled by the equation

$$y = a \cdot \exp(t/\tau_1) + b \cdot \exp(t/\tau_2) + c \qquad (5)$$

fit the data extremely well (R > 0.98), while a single exponential did not fit the data satisfactorily as it only fit the curve for either short or long times. The two relaxation times have mean values of 2.9 ± 2.0 and 56 ± 45 s.

Another function, that may be used to fit the stress relaxation data is the stretched exponential function, also known as the Kohlrausch decay model,

$$y = a \cdot \exp(-(t/\tau)^{\beta}) \qquad (6).$$

This function also fit the data well, with no statistical difference in accuracy of fit between it and the double exponential curve. The stretched exponential model assumes a continuous distribution of relaxation rates, as opposed to the two rates given by the double exponential [20]. The average values for τ and β are 98.1 ± 173.6 s and 0.43 ± 0.24.

Fibrinogen Secondary Structure

Electrospinning fibrinogen fibers requires a very high protein concentration (80 mg/ml or higher), and it usually also requires a volatile, fluorinated hydrocarbon solvent, such as HFP. It is known that such solvents induce α-helical structure in proteins [21]. We performed circular dichroism spectroscopy to determine the difference in secondary structures of fibrinogen in aqueous buffers and in 96.7% HFP (Fig. 8). As expected, fibrinogen has a higher alpha-helical content in HFP (gold curve), than in aqueous buffer (black curve). Estimates of fibrinogen's helix content in PBS (31-37%) and HFP (53-63%) were obtained from the $[\Theta_{220}]$ values measured in each solvent, using calibration parameters of $[\Theta_{220}] \sim -37000$ to -44000 deg cm^2 dmol^{-1} for a 100% helical polypeptide chain, as described by Bulheller [22].

Discussion

We have developed a combined atomic force microscope (AFM) /inverted optical microscope technique to study the mechanical and viscoelastic properties of nanoscopic fibers. The range of forces that could be applied with this technique, using a range of

standard, commercially available cantilevers, covers six orders of magnitude from F = 10^{-2} nN to 10^4 nN. Many biological fibers range in radii from a few to several hundred nanometers and in elastic moduli from E = 10^6 Pa to 10^9 Pa (table 1). Thus, the forces needed to investigate those fibers, $F = E \cdot A \cdot \varepsilon$, where A is the cross-sectional area of the fibers and ε is the strain, are in the range of 10^{-2} to 10^4 nN, which is perfectly covered by this technique. Few other techniques will be able to cover this force range so well. The maximum force in laser tweezers is about 0.15 nN [23] and in AFM normal force measurements the stretching process cannot be easily observed and the maximum force is limited by the substrate-sample and tip-sample bonds, which are typically on the order of a few nN [24]. Moreover, the set-up of our technique also provides a well-defined and easy-to-analyze geometry for longitudinal stress-strain measurements.

We have used this technique to determine several key mechanical properties of electrospun fibrinogen fibers. We studied these fibers, because they may form the basis for numerous medical and material science applications. Our data may be used to design fibrinogen fiber structures with predictable mechanical properties.

We found that electrospun fibrinogen fibers can be extended to 2.3 times their length, (ε_{max} = 1.3), and that the breaking stress is 22 MPa. Electrospun fibrinogen fibers also display clear viscoelastic properties, as they show stress relaxation when held at constant strain. The stress relaxation data of electrospun fibrinogen fibers can be fit very well with a double exponential model, yielding two relaxation times of 3 s and 56 s. The average total stretch modulus, at a pulling speed of 340 nm/s, is $16 \cdot 10^6$ Pa; the elastic modulus (after relaxation) is $6.7 \cdot 10^6$ Pa. Electrospun fibrinogen fibers show some strain softening as the total and elastic moduli decrease with increasing strain.

It is interesting to compare the properties of electrospun fibrinogen fibers to the properties of other, natural fibers (table 1, more extensive table, see [25]). Biological fibers can generally be divided into two groups: 1) Soft, extensible fibers with a Young's modulus on the order of MPa and extensibility, ε_{max}, larger than 1 (can be stretched to at least twice their length). Members of this group are elastin fibers, resilin fibers, intermediate fibers, fibrillin fibers, fibronectin and the extremely stretchable, natural fibrin fibers. 2) Stiffer, less extensible fibers with an about 1000 times larger stiffness on the order of GPa and an extensibility smaller than 0.2. Members of this group are collagen fibers, actin filaments and microtubules. Electrospun fibrinogen fibers clearly fall in group 1 (soft and extensible).

It is also interesting to compare the properties of electrospun fibrinogen fibers more closely with the properties of naturally formed fibrin fibers, because they share the same building block. The alpha helical content of human fibrinogen in PBS, as determined here by CD spectroscopy, was 31-37%. This is consistent with crystallographic data indicating 30% helix content for chicken fibrinogen [30]. Chicken fibrinogen displays strong sequence homology to the human and bovine proteins; however, it lacks the long, flexible α-chain C-terminal domain [17]. Most of the alpha-helical content of fibrinogen is located in the coiled coils spanning the E- and D-domain (see Fig. 1). The alpha helical content of human fibrinogen increased to 53-63% in HFP. The location of this additional, HFP-induced alpha-helical structure in fibrinogen is not known. We speculate that it may be in the large, mainly unstructured α-chain C-terminal domain. Conversion of this domain would be minimally disruptive to the rest of the well-defined structure of fibrinogen, which is stabilized by 29 disulfide bonds.

The properties of fibrin fibers have been recently investigated [14, 26]. Partially crosslinked and non-crosslinked fibrin fibers have a large extensiblity (ε_{max} = 3.3 and 2.3, respectively); crosslinked and non-crosslinked fibrin fibers have an elastic modulus of about 15 MPa and 2 MPa, respectively. Thus, it appears that the mechanical properties of naturally formed fibrin fibers and electrospun fibrinogen fibers are somewhat similar, despite the fact that fiber formation is very different. Natural fibrin fibers are linked together by very specific bonds; in non-crosslinked fibers, these are the A:a knob-hole interactions. The two A knobs, which are exposed after thrombin cleavage of peptide A, located in the central domain of fibrin bind to the a-holes in the end domain of two adjacent fibrin molecule. This results in the regular, half-staggered arrangement of fibrin molecules to form a fibrin fiber. In crosslinked fibrin fibers, activated factor XIII forms longitudinal crosslinks (the (γ–γ crosslinks) across the abutting end domains of two fibrin molecules and lateral crosslinks (α–α crosslinks) between adjacent fibrin molecules in the radial direction [17].

It is unknown which specific molecular interactions hold electrospun fibrinogen molecules together, though it is clear that they are different from the A:a interactions and the crosslinking formed in natural fibrin fibers. The A knob is not available because no thrombin was added to remove fibrinopeptide A; and no crosslinks are formed under our electrospinning conditions (as analyzed by SDS PAGE, data not shown). Electrospun fibrinogen fibers are probably just held together by numerous non-specific interactions. Also, electrospun fibers are formed in dry conditions. The solvent must evaporate from the protein solution before the protein solution reaches the grounding plate during electrostatic spinning. The dried fibers are then rehydrated.

Since both electrospun fibrinogen and natural fibrin fibers show somewhat similar mechanical properties, but assemble in a very different way, it is likely that the underlying building block, fibrin(ogen), influences the mechanical properties of the whole fiber to a large extent. This, then suggests that it should certainly be possible to electrospin fibers with different, and somewhat predictable, mechanical properties by using and mixing molecular building blocks with different properties.

Two underlying molecular mechanisms by which fibrin fibers can achieve their remarkably large extension and elasticity [14] have recently been proposed: an extension of the alpha-helical coiled coils to beta strands, and a partial unfolding of the globular D-domains of the fibrin monomer [25, 27-29]. This two-step model is consistent with recent experimental findings. It is consistent with the observation that fibrinogen lengthens to twice its length at about 100 pN applied force. This lengthening is attributed to the alpha helical to beta strand conversion of the coiled coils [28, 29]. Partial unfolding of the D-domain was invoked to explain single molecule unfolding experiments on fibrinogen [27].

We propose that these two underlying molecular extension mechanism (alpha helical to beta strand conversion of coiled coils, and partial unfolding of D-domain of the underlying building block, fibrinogen) are also taking place in electrospun fibrinogen fibers. It would most straightforwardly explain the similar mechanical behavior of the two fibers.

McManus et al. tested the bulk mechanical properties of wet, non-woven mats made from electrospun fibrinogen fibers. The fibers in the mats were randomly oriented, i.e. not aligned in a particular direction. These mats had an extensibility, ε_{max}, of 1.0 – 1.4 and an

elastic modulus of 0.4 – 0.6 MPa [18]. Thus, the extensibilities of the mats and the single fibers are similar; however, both the peak stress and the modulus of elasticity are about an order of magnitude lower for the mats, as compared to single fibers. These comparisons make it clear that the mechanical properties of the mats are a complex combination of the mechanical properties of the single fibers comprising the mats, and several other factors. These other factors include: 1) Void space. The mats contain a large amount of void space which will result in a smaller elastic modulus. 2) Fiber Alignment. Since the fibers in the mats are initially not aligned, stretching of the mats may first align the fibers in the stretch direction before the individual fibers are stretched. Since aligning of the fibers likely requires less force than stretching them, this aligning mechanism would lower the elastic modulus for the mats. It would also increase the extensibility of the mats. 3) Fiber connections. The properties of the connections between fibers will influence the mechanical performance of the mats; for example, weak connections would result in a reduced elastic modulus, peak stress and extensibility for the mats. 4) Fiber entanglement. More entanglement would strengthen the mats and likely result in a larger elastic modulus for the mats.

These considerations indicate that the properties of macroscopic structures depend in a complex way on the properties of its individual constituents (fibers), the connections between its constituents and the underlying architecture. In future work we will attempt to unravel the contributions of each of these components to the properties of the overall macroscopic structure. This can be done by combining microscopic testing, as done in our paper, macroscopic testing, and finite element modeling to combine the microscopic and macroscopic properties. Such experiments should make it possible to design macroscopic structures with desirable properties, starting with the properties of the microscopic fibers and the connections between them. One key application would be designing, modeling and testing scaffolds for cells in tissue engineering. Cells are extremely sensitive to the mechanical, architectural and chemical properties of the scaffolds and the underlying fibers. In the future we will also test fibers spun from different natural and synthetic materials (e.g. fibrinogen, collagen and mixtures) and evaluate their performance in tissue scaffolds.

Conclusions

We have developed a combined microscopy technique to study the mechanical properties of nanoscopic fibers and used it to investigate electrospun fibrinogen fibers. The mechanical properties of these fibers are important for numerous applications in tissue engineering as well as polymer composites and biomimetics. As compared to other biological protein fibers, electrospun fibrinogen fibers have a low modulus and a high extensibility. However, the electrospun fibrinogen fibers are not quite as soft and extensible as their naturally formed counterpart, fibrin fibers.

Acknowledgments

This work was supported by grants from the NSF (M.G., CMMI-0646627), Wake Forest University (M.G. & R.R.H., Cross-campus grant) and an American Heart Association pre-doctoral fellowship (C.R.C., 081503E).

Figure Captions

Figure 1 (A) Crystal structure of chicken fibrinogen [30]. The monomer is 45 nm long and composed of six polypeptide chains, two alpha chains labeled with gray, two beta chains labeled with black and two gamma chains labeled with gold. Bovine fibrinogen [31], used in our electrospinning experiments, is highly homologous and structurally very similar to chicken fibrinogen, except for the flexible α-chain C-terminal domain, which chicken fibrinogen lacks. **(B)** Schematic of the electrospinning setup. At the top, a syringe pump is used to regulate the flow of the polymer solution (green) from of the syringe. The needle of the syringe is charged to a high potential using a voltage supply. At the bottom left, the fibers being produced from the syringe are collected on the substrate.

Figure 2 (A) Photograph of the experimental setup, the AFM sitting on top of the inverted optical microscope. **(B)** Schematic of the experimental setup. The AFM tip is used to stretch fibers that are suspended over the grooves of a striated substrate. **(C)** Schematic top view. L_{init} is the initial length and L' the length of the stretched fiber. Using trigonometry, L' can be calculated from the initial length and the tip travel, s. It can also be directly measured from the optical image. **(D)** Fluorescence microscopy movie frames of a stretching experiment. The fiber is anchored on two ridges (8 μm wide bars) and suspended over a groove (12 μm wide bar); the AFM cantilever appears as a faintly visible 35 μm shadow. The position of the AFM tip is marked with an asterisk (*).

Figure 3 Schematic view of the AFM laser reflecting off the cantilever and hitting the photodiode. **(A)** The alignment of the laser on the photodiode before contacting the fiber. **(B)** The alignment of the laser on the photodiode after contact of the cantilever with the fiber. The force of the fiber causes the cantilever to twist by an angle, θ, and therefore changes the angle at which the laser hits the photodiode, resulting in a changed left-right photocurrent.

Figure 4 (A) An AFM image of an electrospun fibrinogen fiber on a glass substrate. The color scale on the left corresponds to height. **(B)** A Cross-section taken along the horizontal black line through the AFM image in A. The diameter is measured from the cross section by looking at the z height difference between two points, one along the background and one at the top of the fiber. The diameter of this fiber is 120nm. **(C)** A 50 x 50 μm AFM scan of multiple electrospun fibrin fibers on glass.

Figure 5 (A-D) Fluorescence microscopy movie frames of an electrospun fibrinogen fiber manipulation. The fiber is suspended from two ridges over a groove. The position of the AFM tip is marked with an asterisk (*). This fiber ruptured at the ridge in frame D. **(E)** Maximum extensibility of the hydrated electrospun fibrinogen fibers (N = 34 data points). The average maximum extensibility, ε_{max}, was 1.3. **(F)** Maximum stress, σ_{max}, at which hydrated electrospun fibrinogen fibers ruptured. The average maximum stress at which the fibers broke was 22 MPa. The range of the x axis in E and F is determined by the lowest and highest measured values, and divided into $N^{1/2}$ bins.

Figure 6 (A) Strain versus times curve for an incremental fiber manipulation. During incremental manipulations the fibers were stretched forward and then held at a given strain (plateau regions of the curve) giving the fiber time to relax. **(B)** Stress versus time curve for an incremental fiber manipulation. The stress decays exponentially during the time period when the fiber is being held at a given strain. The decay indicates the electrospun fibrinogen fibers are viscoelastic. **(C)** Incremental stress versus strain for an electrospun fibrinogen fiber. The gold curve is the raw data for the fiber, the solid black line is the total modulus given by determining the slope between adjacent peaks, and the dashed black line is the elastic component of the total modulus. The elastic component is determined from fitting the exponential relaxations curves and again connecting adjacent relaxation minimums.

Figure 7 Individual relaxation curve for an electrospun fibrinogen fiber. The curve is fit with a double exponential curve, producing two characteristic relaxation times for the fiber. For this fiber the fast relaxation time, τ_1, is 4.0 s and the slow relaxation time, τ_2, is 53 s.

Figure 8 (A) CD Spectra of fibrinogen in phosphate-buffered saline (PBS, solid black line) and spin solvent, hexafluoro -2-propanol (HFP, gold line). **(B)** CD spectra of pure alpha-helical, beta-I and beta-II configurations (Image from: Bulheller, [22] – reproduced by permission of the PCCP Owner Societies). It is apparent that fibrinogen remains largely folded in the spin solvent; and that its alpha-helical content increases upon transfer to the spin solvent.

Tables

Material	E (MPa)	ε_{max}
High extensibility, soft fibers		
Electrospun fibrinogen fibers	7	1.3
Crosslinked[a], uncrosslinked[b] , partially crosslinked[c] fibrin fibers	15[a], (2)[b]	3.3[c], (2.3)[b]
Elastin (Bovine ligament)	1	1.5
Resilin (dragonfly tendon[d], cloned[e])	1-2[d]	1.9[a] , 3.1[e]
Matrix-free Intermediate filament (mammalian[f], hagfish[g])	6-300[f]	1.6[c] , 2.2[g]
Fibrillin	0.2 – 100	> 1.9
Fibronectin	-	2.0 – 3.0
Myofibrils (sarcomere), titin (connectin))	1	2.0
Low extensibility, stiff fibers		
Tendon collagen (mammalian tendon)	160-7,500	0.12
Actin	1,800-2,500	≤ 0.15
Microtubules	1,000-1,500	≤ 0.20

Table 1 (adapted from [25]). Stiffness (Young's modulus, E) and breaking strain (extensibility ε_{max}) of various protein fibers. There are two reasons for the range of values in the Young's modulus of a given fiber: 1) Authors report a range of values. 2) Strain hardening/softening; the fibers become stiffer/softer as the strain increases.

References

1. Doolittle RF. Fibrinogen and Fibrin. Annual Review of Biochemistry 1984;53:195-229.
2. Ferry JD. The mechanism of polymerization of fibrin. Proc Natl Acad Sci U S A 1952;38:566-569.
3. Ryan EA, Mockros LF, Weisel JW, Lorand L. Structural Origins of Fibrin Clot Rheology. Biophysical Journal 1999;77:2813-2826.
4. Hemostasis and Thrombosis. Basic Principles and Clinical Practice. 4th ed. Philadelphia, PA: Lippincott Williams & Wilkins, 2001.
5. Huang Z-M, Zhang YZ, Kotaki M, Ramakrishna S. A review on polymer nanofibers by electrospinning and their applications in nanocomposites. Composites Science and Technology 2003;63(15):2223-2253.
6. Kim JS, Reneker DH. Mechanical properties of composites using ultrafine electrospun fibers. Polymer Composites 1999;20(1):124-131.
7. Ye Q, Zund G, Benedikt P, Jockenhoevel S, Hoerstrup SP, Sakyama S, et al. Fibrin gel as a three dimensional matrix in cardiovascular tissue engineering. European Journal of Cardio-Thoracic Surgery 2000;17(5):587-591.
8. Bootle-Wilbraham CA, Tazzyman S, Thompson WD, Stirk CM, Lewis CE. Fibrin fragment E stimulates the proliferation, migration and differentiation of human microvascular endothelial cells in vitro. Angiogenesis 2001;4(4):269-275.
9. Dvorak HF, Harvey VS, Estrella P, Brown LF, McDonagh J, Dvorak AM. Fibrin containing gels induce angiogenesis. Implications for tumor stroma generation and wound healing. Lab Invest 1987;57:673-686.
10. McManus MC, Boland ED, Simpson DG, Barnes CP, Bowlin GL. Electrospun fibrinogen: Feasibility as a tissue engineering scaffold in a rat cell culture model. Journal of Biomedical Materials Research Part A 2007;81A(2):299-309.
11. McManus M, Boland E, Sell S, Bowen W, Koo H, Simpson D, et al. Electrospun nanofibre fibrinogen for urinary tract tissue reconstruction. Biomedical Materials 2007;2(4):257-262.
12. Xia YN, Whitesides GM. Soft Lithography. Angewandte Chemie - Intl Ed 1998;37(5):551-575.
13. Wnek GE, Carr ME, Simpson DG, Bowlin GL. Electrospinning of nanofiber fibrinogen structures. Nano Letters 2003;3(2):213-216.
14. Liu W, Jawerth LM, Sparks EA, Falvo MR, Hantgan RR, Superfine R, et al. Fibrin Fibers Have Extraordinary Extensibility and Elasticity. Science 2006;313:634.
15. Peng L, Stephens BJ, Bonin K, Cubicciotti R, Guthold M. A combined Atomic Force/Fluorescence Microscopy Technique to Select Aptamers in a Single Cycle from a Small Pool of Random Oligonucleotides. Microscopy Research and Technique 2007;70:372-381.
16. Liu W, Bonin K, Guthold M. An easy and direct method for calibrating AFM lateral force measurements. Rev Sci Instrum 2007;78(6):063707.
17. Hantgan RR, Lord ST. Fibrinogen Structure and Physiology. In: Colman RW, Marder VJ, Clowes AW, George JN, Goldhaber SZ, editors. Hemostasis and Thrombosis Basic Principles and Clinical Practice. 5 ed. Philadelphia: Lippincott Williams and Wilkins, 2006. p. 285-316.

18. McManus MC, Boland ED, Koo HP, Barnes CP, Pawlowski KJ, Wnek GE, et al. Mechanical properties of electrospun fibrinogen structures. Acta Biomaterialia 2006;2(1):19-28.
19. Prescott J. Applied Elasticity. New York: Dover Publications, Inc., 1961.
20. Berberan-Santos MN, Bodunov EN, Valeur B. Mathematical functions for the analysis of luminescence decays with underlying distributions 1. Kohlrausch decay function (stretched exponential). Chemical Physics 2005;315:171-182.
21. Creighton TE. Proteins:Structures and Molecular Properties. 2nd ed. New York: W.H. Freeman and Co., 1993.
22. Bulheller BM, Rodger A, Hirst JD. Circular and linear dichroism of proteins. Physical Chemistry Chemical Physics 2007;9(17):2020-2035.
23. Bustamante C, Macosko JC, Wuite GJL. Grabbing the cat by the tail: Manipulating molecules one by one. Nature Reviews Molecular Cell Biology 2000;1(2):130-136.
24. Grandbois M, Beyer M, Rief M, Clausen-Schaumann H, Gaub HE. How Strong Is a Covalent Bond? Science 1999;283(5408):1727-1730.
25. Guthold M, Liu W, Sparks EA, Jawerth LM, Peng L, Falvo M, et al. A comparison of the mechanical and structural properties of fibrin fibers with other protein fibers. Cell Biochemistry and Biophysics 2007;49(3):165-181.
26. Collet JP, Shuman H, Ledger RE, Lee ST, Weisel JW. The elasticity of an individual fibrin fiber in a clot. Proceedings of the National Academy of Sciences of the United States of America 2005;102(26):9133-9137.
27. Averett LE, Geer CB, Fuierer RR, Akhrernitchev BB, Gorkun OV, Schoenfisch MH. Complexity of "A-a" knob-hole fibrin interaction revealed by atomic force spectroscopy. Langmuir 2008;24(9):4979-4988.
28. Brown AEX, Litvinov RI, Discher DE, Weisel JW. Forced Unfolding of Coiled-Coils in Fibrinogen by Single-Molecule AFM. Biophysical Journal 2007;92:L30 - L41.
29. Lim BBC, Lee EH, Sotomayor M, Schulten K. Molecular basis of fibrin clot elasticity. Structure 2008;16(3):449-459.
30. Yang Z, Kollman JM, Pandi L, Doolittle RF. Crystal structure of native chicken fibrinogen at 2.7 angstrom resolution. Biochemistry 2001;40(42):12515-12523.
31. Brown JH, Volkmann N, Jun G, Henschen-Edman AH, Cohen C. The crystal structure of modified bovine fibrinogen. Proceedings of the National Academy of Sciences of the United States of America 2000 Jan 4;97(1):85-90.

A

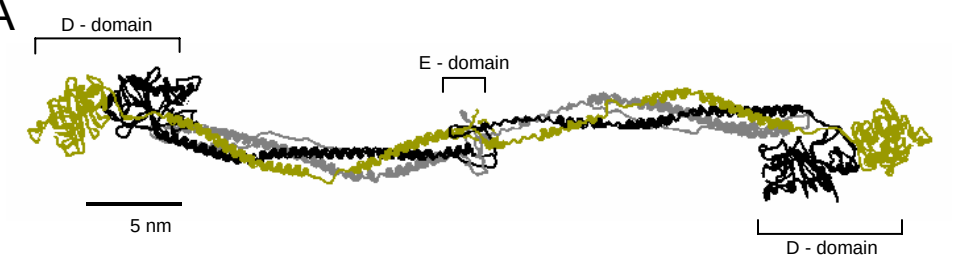

B

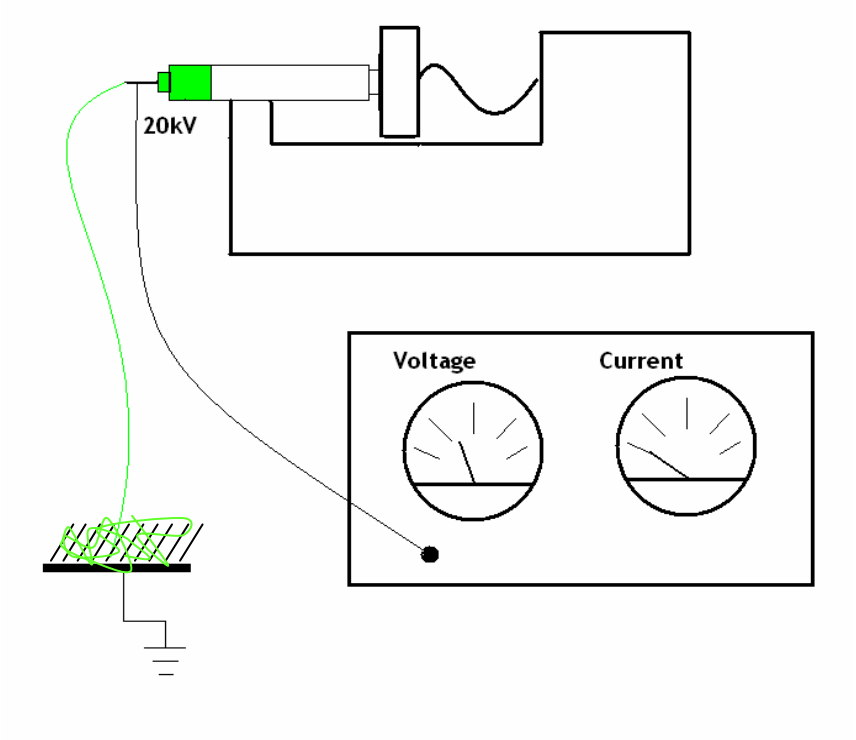

A

B

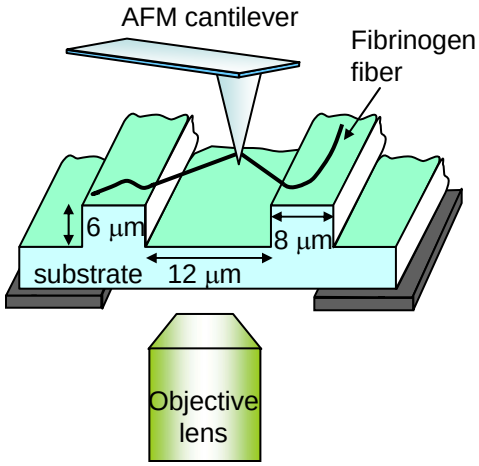
AFM cantilever
Fibrinogen fiber
6 μm
8 μm
substrate
12 μm
Objective lens

C

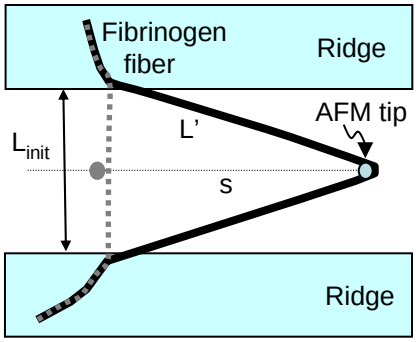
Fibrinogen fiber
Ridge
AFM tip
L'
L_{init}
s
Ridge

D

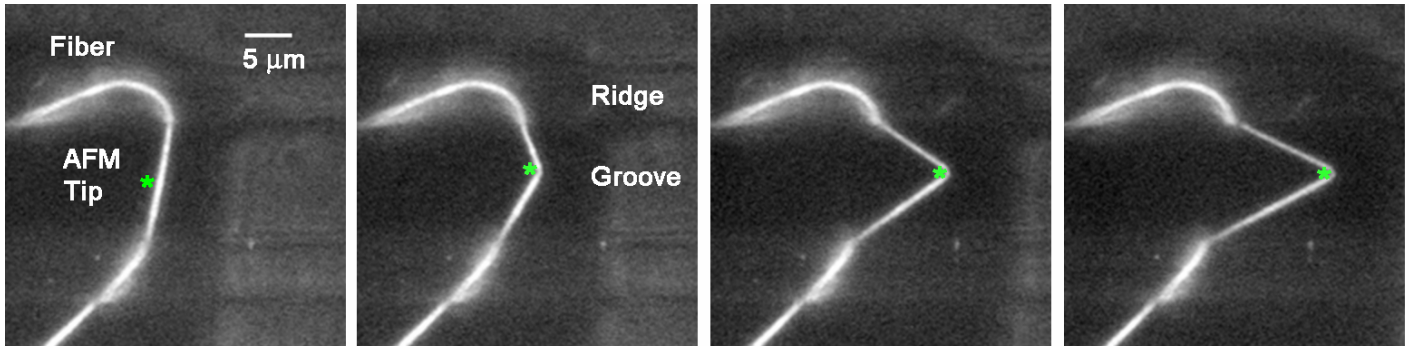
Fiber
5 μm
AFM Tip
Ridge
Groove

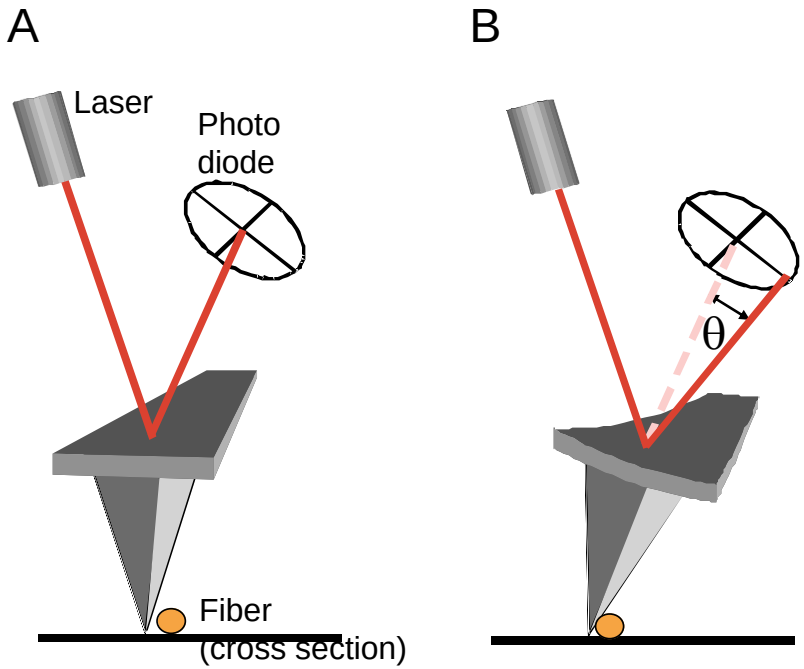
A
Laser
Photo
diode
Fiber
(cross section)
B
θ

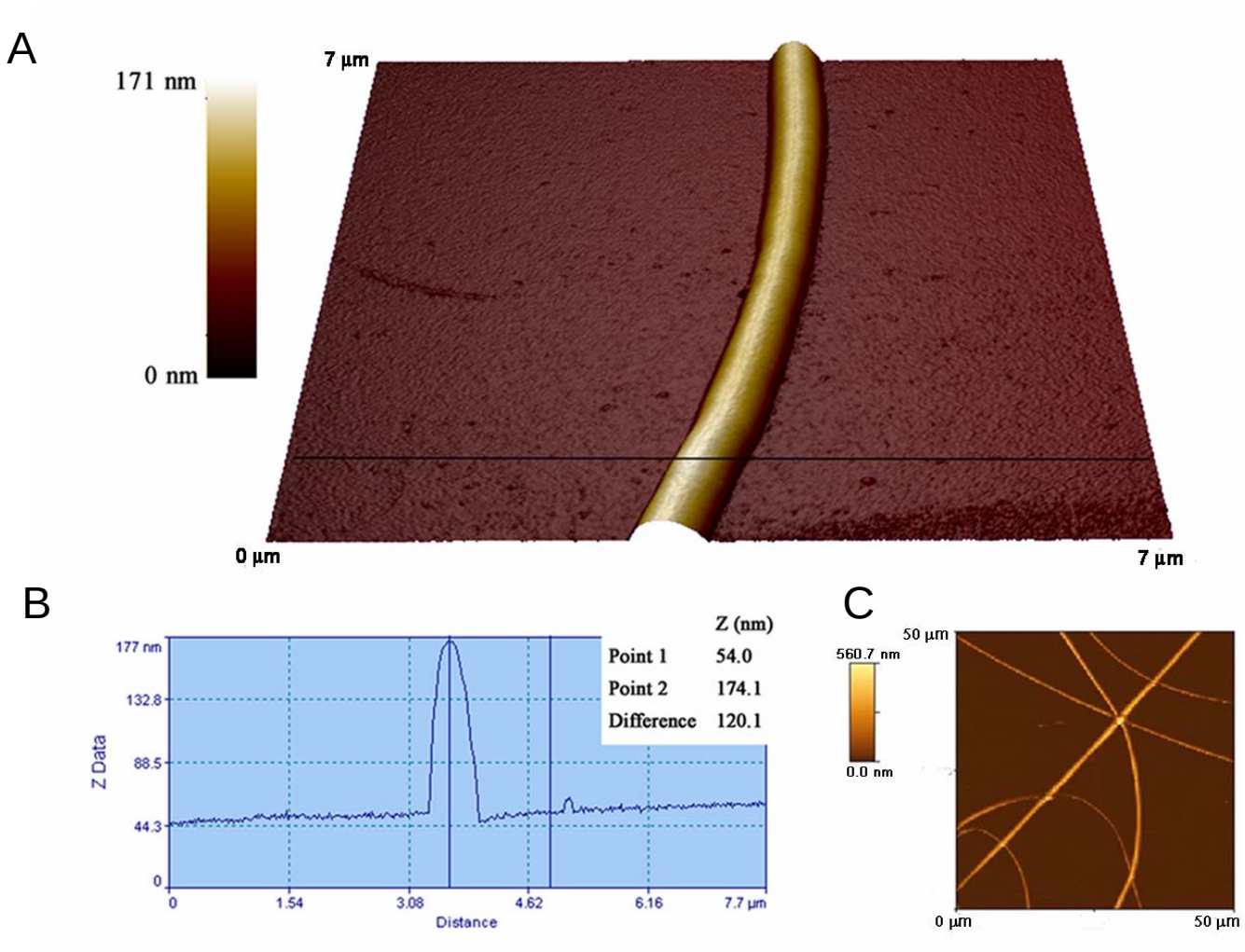
A
171 nm
0 nm
7 µm
0 µm
7 µm
B
Z (nm)
Point 1 54.0
Point 2 174.1
Difference 120.1
177 nm
132.8
88.5
44.3
0
Z Data
0
1.54
3.08
4.62
6.16
7.7 µm
Distance
C
50 µm
560.7 nm
0.0 nm
0 µm
50 µm

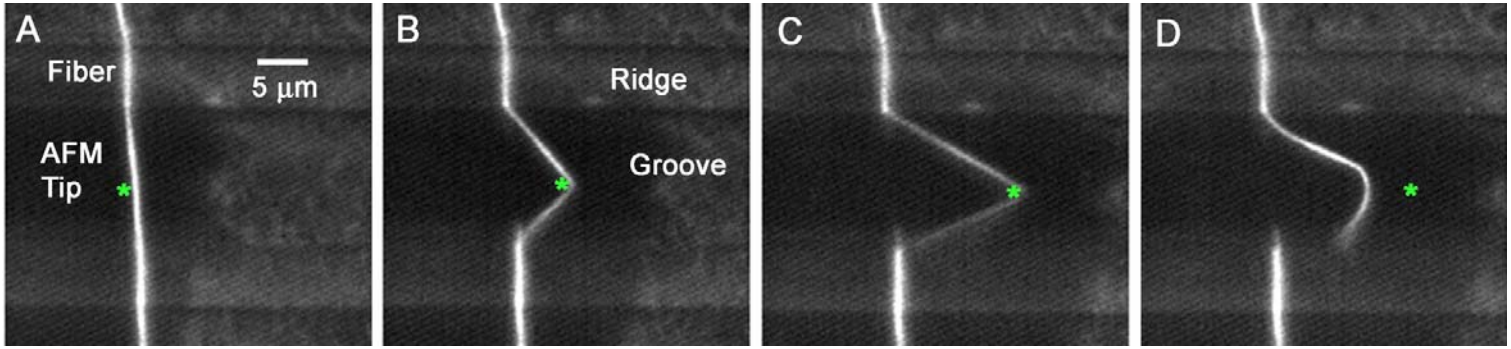
A
Fiber
5 µm
AFM
Tip
B
Ridge
Groove
C
D

E

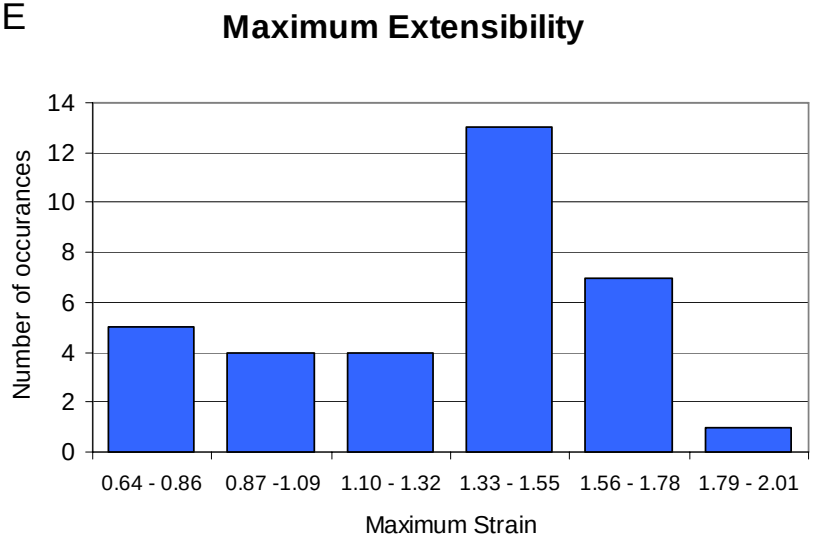
Maximum Extensibility
Number of occurances
0
2
4
6
8
10
12
14
0.64 - 0.86
0.87 -1.09
1.10 - 1.32
1.33 - 1.55
1.56 - 1.78
1.79 - 2.01
Maximum Strain

F

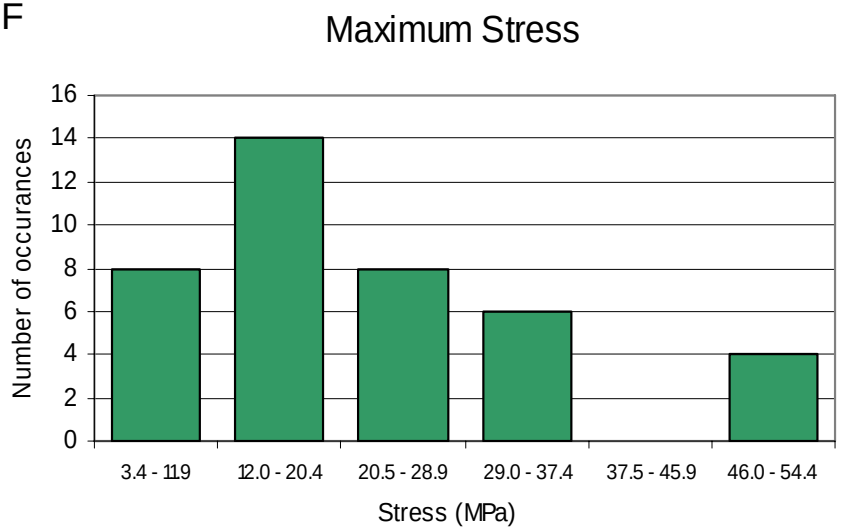
Maximum Stress
Number of occurances
0
2
4
6
8
10
12
14
16
3.4 - 11.9
12.0 - 20.4
20.5 - 28.9
29.0 - 37.4
37.5 - 45.9
46.0 - 54.4
Stress (MPa)

A

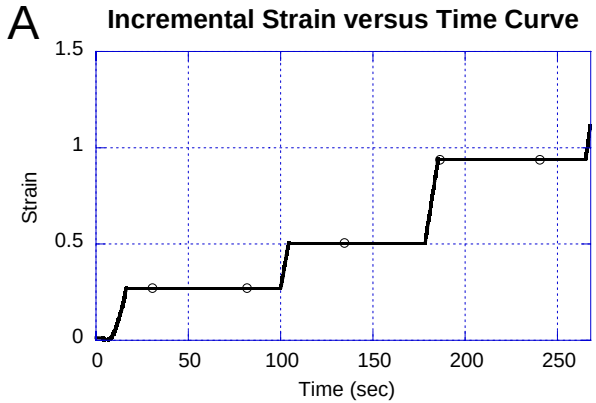
Incremental Strain versus Time Curve
Strain
Time (sec)
0
0.5
1
1.5
0
50
100
150
200
250

B

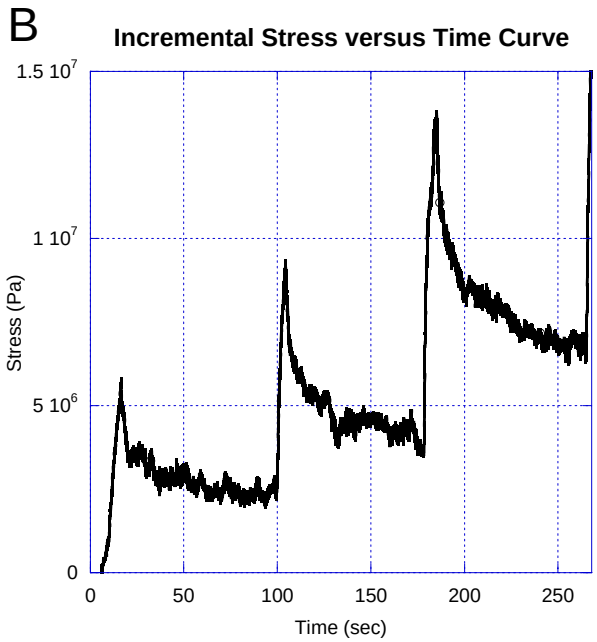
Incremental Stress versus Time Curve
Stress (Pa)
Time (sec)
0
5 10^6
1 10^7
1.5 10^7
0
50
100
150
200
250

C

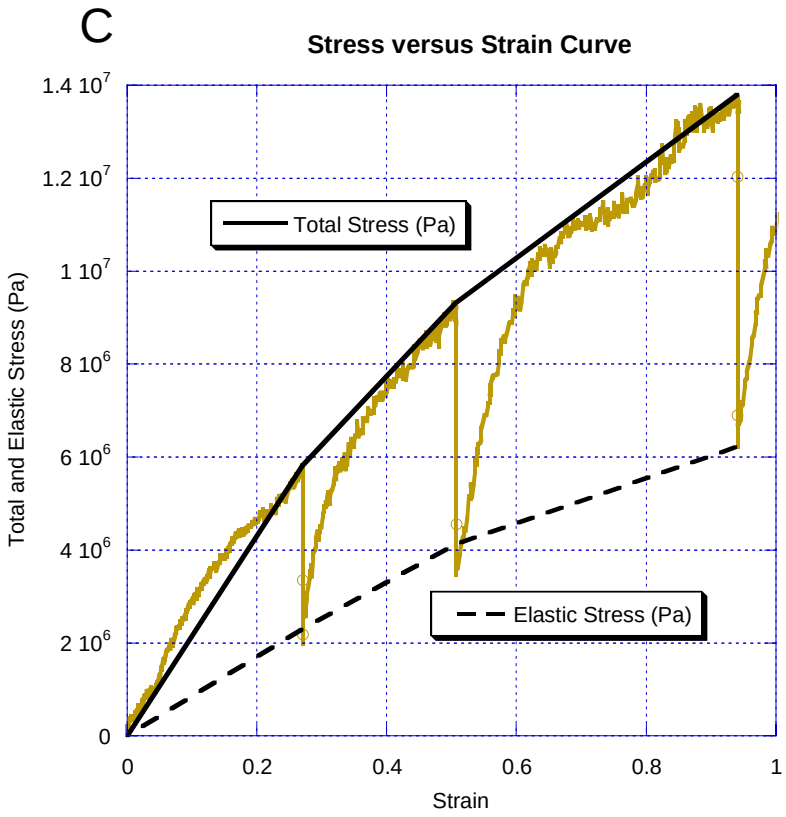
Stress versus Strain Curve
Total and Elastic Stress (Pa)
Strain
Total Stress (Pa)
Elastic Stress (Pa)
0
2 10^6
4 10^6
6 10^6
8 10^6
1 10^7
1.2 10^7
1.4 10^7
0
0.2
0.4
0.6
0.8
1

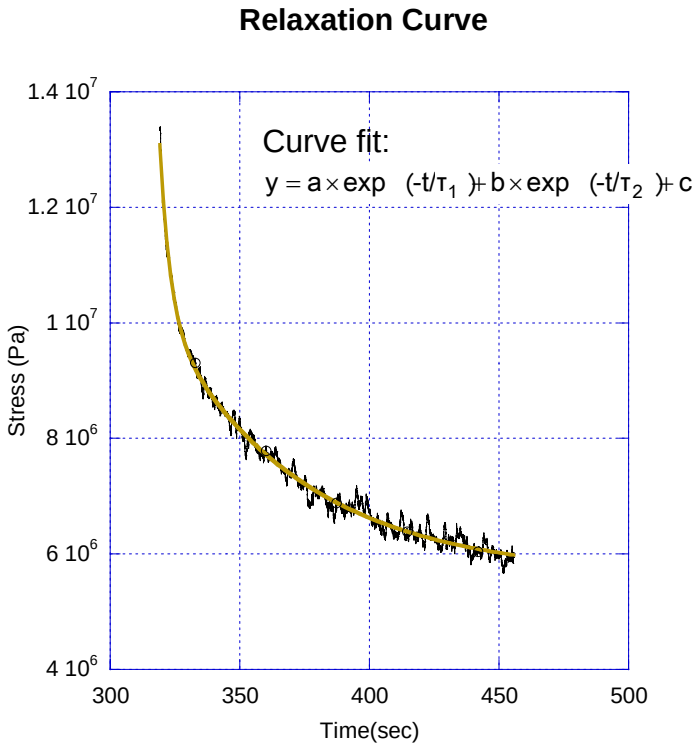
Relaxation Curve
Curve fit:
y = a × exp (-t/τ1) + b × exp (-t/τ2) + c
1.4 10^7
1.2 10^7
1 10^7
8 10^6
6 10^6
4 10^6
Stress (Pa)
300
350
400
450
500
Time(sec)

A

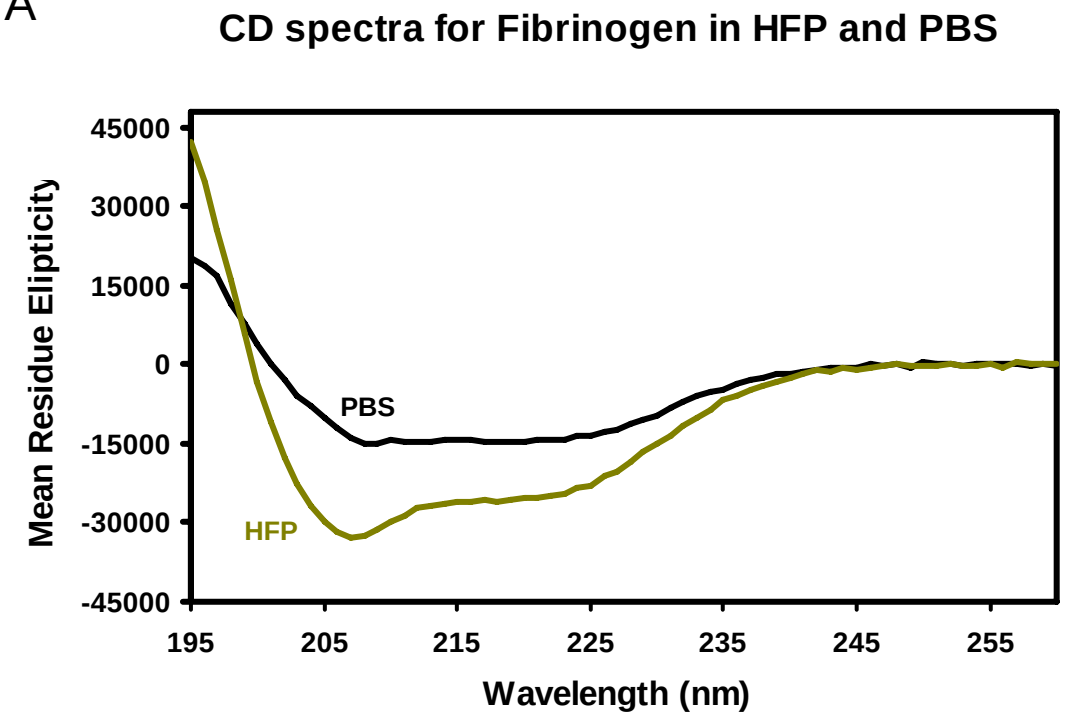
CD spectra for Fibrinogen in HFP and PBS
Mean Residue Elipticity
45000
30000
15000
0
-15000
-30000
-45000
195
205
215
225
235
245
255
Wavelength (nm)
PBS
HFP

B

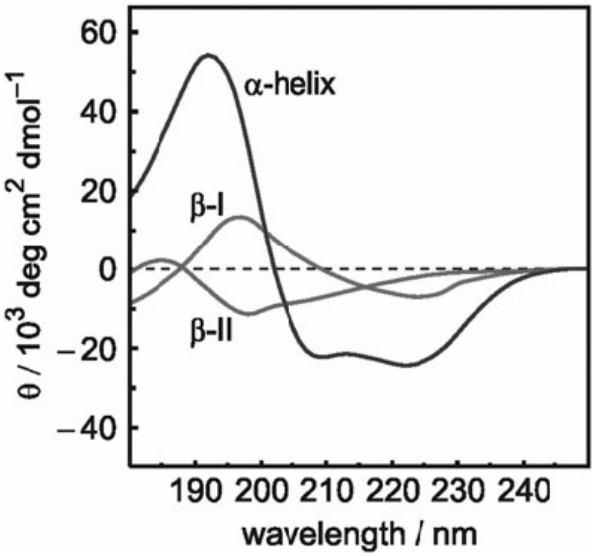
θ / 10^3 deg cm^2 dmol^-1
60
40
20
0
−20
−40
α-helix
β-I
β-II
190 200 210 220 230 240
wavelength / nm